

Numerical study of $O(a)$ improved Wilson quark action on anisotropic lattice

Hideo Matsufuru¹, Tetsuya Onogi¹ and Takashi Umeda²

¹*Yukawa Institute for Theoretical Physics, Kyoto University,
Kyoto 606-8502, Japan*

²*Center for Computational Physics, University of Tsukuba,
Tsukuba 305-8577, Japan*

30 June 2001

Abstract

The $O(a)$ improved Wilson quark action on the anisotropic lattice is investigated. We carry out numerical simulations in the quenched approximation at three values of lattice spacing ($a_\sigma^{-1} = 1-2$ GeV) with the anisotropy $\xi = a_\sigma/a_\tau = 4$, where a_σ and a_τ are the spatial and the temporal lattice spacings, respectively. The bare anisotropy γ_F in the quark field action is numerically tuned by the dispersion relation of mesons so that the renormalized fermionic anisotropy coincides with that of gauge field. This calibration of bare anisotropy is performed to the level of 1 % statistical accuracy in the quark mass region below the charm quark mass. The systematic uncertainty in the calibration is estimated by comparing the results from different types of dispersion relations, which results in 3 % on our coarsest lattice and tends to vanish in the continuum limit. In the chiral limit, there is an additional systematic uncertainty of 1 % from the chiral extrapolation.

Taking the central value $\gamma_F = \gamma_F^*$ from the result of the calibration, we compute the light hadron spectrum. Our hadron spectrum is consistent with the result by UKQCD Collaboration on the isotropic lattice. We also study the response of the hadron spectrum to the change of anisotropic parameter, $\gamma_F \rightarrow \gamma_F^* + \delta\gamma_F$. We find that the change of γ_F by 2 % induces a change of 1 % in the spectrum for physical quark masses. Thus the systematic uncertainty on the anisotropic lattice, as well as the statistical one, is under control.

1 Introduction

The anisotropic lattice is drawing more attention as a useful technique of the lattice QCD simulation in various physics such as the spectroscopy of exotic states, finite temperature QCD and the heavy quark physics. However, the advantage of having a fine lattice spacing in the temporal direction is obtained at the sacrifice of manifest temporal-spatial axis-interchange symmetry. Therefore improper use of the anisotropic lattice could lead to an unphysical result due to the lack of Lorentz symmetry in the continuum limit. This can be a serious problem for those physics in which the precision of the results is crucial.

One way to avoid this problem is to tune the anisotropy parameters of the action by imposing the conditions with which the Lorentz invariance is satisfied for some physical observables.

In the Wilson plaquette gauge action there is only one anisotropic parameter in the action [1]. Wilson loops are used to obtain the relation between the anisotropic parameter and the physical ratio of the lattice spacings in temporal and spatial directions, $\xi = a_\sigma/a_\tau$, where a_σ and a_τ are the spatial and the temporal lattice spacings [2, 3, 4, 5]. On the other hand, not much is known about the quark action. This is because the previous works with the quark action on the anisotropic lattice have been devoted to the charmonium systems [6, 7, 8, 9]. In order to apply the anisotropic lattice to the systems containing the light quarks, one has to study how one can tune the parameter of light quark action in practical simulations.

In this paper we study the $O(a)$ improved Wilson action on the anisotropic lattice using the quenched lattices with three lattice spacings, at fixed renormalized anisotropy, $\xi = 4$. These scales covers the range of the spatial lattice cutoff $a_\sigma^{-1} = 1-2$ GeV. We first tune the bare anisotropy in the quark action numerically so that the renormalized fermionic anisotropy is equal to that of the gauge field by imposing the relativistic dispersion relation of mesons. This calibration is performed to the level of 1 % statistical accuracy in whole quark mass region below the charm quark mass. The extrapolation of tuned bare anisotropy to the chiral limit is performed by fitting to presumable forms, and causes additional systematic uncertainty of 1 % at the chiral limit. The systematic uncertainty in the calibration from the lattice artifact is estimated by comparing the results from different types of dispersion relations. It results in 3 % on our coarsest lattice, and tends to vanish in the continuum limit. Using the result of the calibration we compute the light hadron spectrum on anisotropic lattices, and examine how the uncertainty in the calibration affect the spectrum at the parameters of physical interest. It is found that the uncertainty of 2 % in calibration induces systematic error of 1 % in the spectrum. Thus the systematic uncertainty on the anisotropic lattice is under control, as well as the statistical one. We also show that the anisotropic lattices produce consistent results with those on the isotropic lattices, and that the Lorentz invariance of the simple matrix element is satisfied within errors.

This paper is organized as follows. The next section describes the $O(a)$ improved Wilson quark action, which has been discussed in [10, 6]. The calibration procedures are discussed in Section 3. In Section 4, we perform the calibration of the bare anisotropy in the quark action. The systematic uncertainty induced by this tuning is fully examined. In Section 5 we apply the anisotropic lattice to the light hadron spectroscopy. In the last part of this section, the systematic uncertainty due to the anisotropy is again investigated in terms of the effect on hadron spectrum. The last section is devoted to our conclusions.

2 Quark action on the anisotropic lattice

2.1 Quark field action

We employ the $O(a)$ improved quark action on the anisotropic lattice. The form of action has been discussed in Ref. [10], which is the same as the Fermilab action [11] but defined on the anisotropic lattice. In this section we summarize the result which will be necessary in the following calculations.

The quark action is represented in the hopping parameter form as

$$S_F = \sum_{x,y} \bar{\psi}(x) K(x,y) \psi(y), \quad (2.1)$$

$$K(x,y) = \delta_{x,y} - \kappa_\tau \left[(1 - \gamma_4) U_4(x) \delta_{x+\hat{4},y} + (1 + \gamma_4) U_4^\dagger(x - \hat{4}) \delta_{x-\hat{4},y} \right]$$

$$\begin{aligned}
& -\kappa_\sigma \sum_i \left[(r - \gamma_i) U_i(x) \delta_{x+\hat{i},y} + (r + \gamma_i) U_i^\dagger(x - \hat{i}) \delta_{x-\hat{i},y} \right] \\
& -\kappa_\sigma c_E \sum_i \sigma_{4i} F_{4i}(x) \delta_{x,y} - r \kappa_\sigma c_B \sum_{i>j} \sigma_{ij} F_{ij}(x) \delta_{x,y},
\end{aligned} \tag{2.2}$$

where κ_σ and κ_τ are the spatial and the temporal hopping parameters, r is the Wilson parameter and c_E and c_B are the clover coefficients. In principle for a given κ_σ , the four parameters $\kappa_\sigma/\kappa_\tau$, r , c_E and c_B should be tuned so that Lorentz symmetry holds up to discretization errors of $O(a^2)$.

On the anisotropic lattice, the mean-filed values of the spatial link variable u_σ and the temporal one u_τ are different from each other. The tadpole-improvement [12] is achieved by rescaling the link variable as $U_i(x) \rightarrow U_i(x)/u_\sigma$ and $U_4(x) \rightarrow U_4(x)/u_\tau$. This is equivalent to redefine the hopping parameters with the tadpole-improved ones (with tilde) through $\kappa_\sigma = \tilde{\kappa}_\sigma/u_\sigma$ and $\kappa_\tau = \tilde{\kappa}_\tau/u_\tau$. We define the anisotropy parameter γ_F as

$$\gamma_F \equiv \frac{\tilde{\kappa}_\tau}{\tilde{\kappa}_\sigma}. \tag{2.3}$$

At the tadpole-improved tree-level, and for sufficiently small quark mass, the anisotropy γ_F coincides with the cutoff anisotropy $\xi = a_\sigma/a_\tau$.

In this work, we set the coefficients of the spatial part of the Wilson term and the clover coefficients as the tadpole-improved tree-level values, namely,

$$r = \frac{1}{\xi}, \quad c_E = \frac{1}{u_\sigma u_\tau^2}, \quad c_B = \frac{1}{u_\sigma^3} \tag{2.4}$$

and perform a nonperturbative calibration only for γ_F with the meson dispersion relation.

It is useful to define κ

$$\frac{1}{\kappa} \equiv \frac{1}{\tilde{\kappa}_\sigma} - 2(\gamma_F + 3r - 4) \tag{2.5}$$

so that the bare quark mass in the spatial lattice unit, $m_{0\sigma}$, is expressed as

$$m_{0\sigma} = \frac{1}{2} \left(\frac{1}{\kappa} - 8 \right), \tag{2.6}$$

which is analogous to the case of the isotropic lattice.

2.2 Dispersion relation of free quark

In this subsection, we examine the dispersion relation of the free quark on the anisotropic lattice. First the tree-level relation of bare anisotropy with ξ is derived from the condition that the rest mass and the kinetic mass coincide. Then, we discuss how the dispersion relation is distorted at the edge of Brillouin zone due to our choice, $r = 1/\xi$ [6].

From the action (2.2), the free quark propagator satisfies the dispersion relation

$$\cosh E(\mathbf{p}) = 1 + \frac{\bar{\mathbf{p}}^2 + (m_0 + \frac{1}{2} \frac{r}{\gamma_F} \hat{\mathbf{p}}^2)^2}{2(1 + m_0 + \frac{1}{2} \frac{r}{\gamma_F} \hat{\mathbf{p}}^2)}, \tag{2.7}$$

where $\bar{p}_i = \frac{1}{\gamma_F} \sin p_i$, $\hat{p}_i = 2 \sin(p_i/2)$ and $m_0 = m_{0\sigma}/\gamma_F$ is the bare quark mass in the temporal lattice unit. Setting $\mathbf{p} = 0$, Eq. (2.7) gives the rest mass

$$M_1 \equiv E(\mathbf{0}) = \ln(1 + m_0). \tag{2.8}$$

On the other hand, the kinetic mass is defined and obtained as

$$\frac{1}{M_2} \equiv \xi^2 \frac{d^2 E}{dp_i^2} \Big|_{\mathbf{p}=0} = \xi^2 \left(\frac{r}{m_0 + 1} + \frac{\frac{2}{\gamma_F^2}}{m_0(m_0 + 2)} \right). \quad (2.9)$$

Generally the rest mass (2.8) and the kinetic mass (2.9) are different. One can tune the bare anisotropy parameter γ_F so that it gives the same values for the rest and the kinetic masses [11]. Putting the rest and the kinetic masses equal, the anisotropy parameter γ_F is represented with m_0 and r as

$$\frac{1}{\gamma_F} = \sqrt{\left(\frac{rm_0(m_0 + 2)}{4(m_0 + 1)} \right)^2 + \frac{m_0(m_0 + 2)}{2\xi^2 \ln(1 + m_0)}} - \frac{rm_0(m_0 + 2)}{4(m_0 + 1)}. \quad (2.10)$$

For small m_0 , γ_F is expanded in m_0 as

$$\begin{aligned} \frac{1}{\gamma_F} &= \frac{1}{\xi} \left[1 + \frac{1}{2}(1 - r\xi)m_0 + \frac{1}{24}(-1 + 6r\xi + 3r^2\xi^2)m_0^2 \right] \\ &= \frac{1}{\xi} \left[1 + \frac{1}{3}m_0^2 \right] \quad (r = 1/\xi). \end{aligned} \quad (2.11)$$

The m_0 dependence starts with the quadratic term for $r = 1/\xi$, therefore the dependence on the quark mass is small for sufficiently small m_0 . For example, let us consider the case of $a_\tau = 4$ GeV, which corresponds to our coarsest lattice in the simulation. The charm quark mass corresponds to $m_0 \simeq 0.3$ and at this value γ_F is different from ξ only 3 %. Up to this quark mass region, one can expect that the difference of γ_F from ξ is also small in the numerical simulation. This is examined in Section 4.

With our choice of Wilson parameter, $r = 1/\xi$, the action (2.2) leads the smaller spatial Wilson term for the larger cutoff anisotropy ξ . The question is how the contribution of the doubler eliminated by the Wilson term becomes significant for practical value of ξ . In the following argument on this subject, we only treat the case γ_F almost equal to ξ , i.e. the region of m_0 sufficiently smaller than unity. Figure 1 shows the dispersion relation (2.7) for several values of m_0 in the case of $\xi = 4$, which we use in the numerical simulation.

Let us examine the practical case, $a_\sigma^{-1} \simeq 1.0$ GeV, which corresponds to the lowest spatial cutoff of our three lattices. For the light quark mass region, $m_0 = 0.02$ – 0.05 corresponds to 80–200 MeV, and roughly covers the mass region which we use in the hadron spectroscopy in Section 5. $E(\mathbf{p}) - E(0)$ rapidly decrease at the edge of the Brillouin zone, and the height at $z = a/\pi$ is around 400 MeV. For two quarks with momenta $p = \pm a/\pi$, additional energy of doublers is ~ 800 MeV, and is expected to affect not severely on the spectrum and other observables. For higher lattice cutoff, the situation becomes better. Then we regard the doubler contribution is sufficiently small on the lattice we use in the simulation. $m_0 = 0.3$ roughly corresponds to the charm quark mass with $a_\sigma^{-1} \simeq 1$ GeV. In the case of heavy-light hadrons, such as D mesons and Λ_c baryon, the scale of momentum transferred inside hadrons is of the order of Λ_{QCD} , and the same argument for light quark case holds. On the other hand, for the heavy quarkonium, the typical energy and momentum exchanged inside the meson are in the order of mv^2 and mv respectively [13]. For the charmonium, $v^2 \sim 0.3$, then typical scale of the kinetic energy is around 500 MeV. It seems not sufficiently smaller than the two doublers' contribution, and hence one need to choose larger lattice cutoff in the calculation of heavy quarkonium.

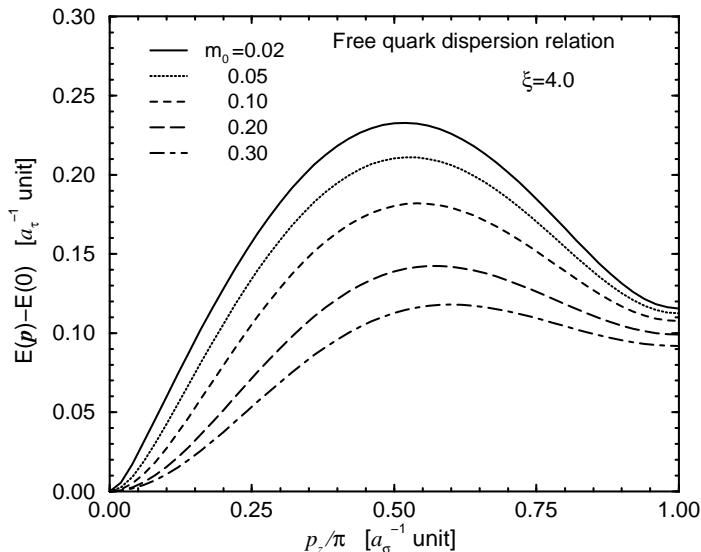


Figure 1: Dispersion relation of the free quark for $\xi = 4$.

3 Calibration procedures

On anisotropic lattice, one must tune the parameters so that the anisotropy of quark field, ξ_F , equals to that of the gauge field, ξ_G :

$$\xi_F(\beta, \gamma_G; \kappa, \gamma_F) = \xi_G(\beta, \gamma_G; \kappa, \gamma_F) = \xi \quad (3.1)$$

Since ξ_G and ξ_F are in general functions of both of gauge parameters (β, γ_G) and quark parameters, (κ, γ_F) , the simulation with dynamical quarks requires to tune these bare parameters simultaneously. In the quenched case, however, this tuning is rather easy to be performed, since ξ_G can be determined independently of γ_F . After the determination of ξ , one can tune γ_F so that a certain observable satisfies the condition (3.1). In this work, we use the relativistic dispersion relation of meson,

$$E^2(\mathbf{p}) = m^2 + \frac{\mathbf{p}^2}{\xi_F^2} + O(\mathbf{p}^4), \quad (3.2)$$

as our main calibration procedure. The energy and the mass of meson, E and m , are in the temporal lattice unit while the momentum is in the spatial lattice unit. The ξ_F appears to convert the momentum in the spatial lattice unit into the temporal lattice unit, and considered as the fermionic anisotropy defined through this relation. With the condition $\xi_F = \xi$, this condition satisfies that the rest mass and the kinetic mass equal to each other. For finite lattice spacings, above dispersion relation only holds up to the $O((\mathbf{p}^2)^2)$ correction term. In the continuum limit, this higher order term in a would vanish and the relativistic dispersion relation would be restored.

In the numerical simulation, we fit E^2 to the form Eq. (3.2) and obtain the value of ξ_F for each input value of bare anisotropy γ_F . Then we linearly interpolate ξ_F in terms of γ_F and find out γ_F^* , the value of γ_F with which $\xi_F = \xi$ holds.

In order to estimate the systematic errors we also use the dispersion relation which corresponds to the lattice Klein-Gordon action [6],

$$\cosh E(\mathbf{p}) - \cosh E(\mathbf{p} = 0) = 1 + \frac{1}{2\xi_{KG}^2} \hat{\mathbf{p}}^2. \quad (3.3)$$

Thus the comparison of these two calibration conditions typically shows the size of the lattice discretization errors.

Expanding this expression in a , ξ_{KG} is related to ξ_F as

$$\xi_{KG} = \xi_F \left(1 - \frac{m^2}{12} + O(a^4) \right). \quad (3.4)$$

The same input γ_F gives smaller value for ξ_{KG} than ξ_F , and therefore the tuned bare anisotropy γ_F^* results in larger value in the former case.

4 Numerical Results of Calibration

The goal of this section is to determine the tuned bare anisotropy of quark field, γ_F^* , at each fixed quark mass in the region from strange to charm quark masses. The reason for this choice of the quark mass range is that the simulation is easier which saves the amount of work in the exhaustive study for calibrations. Fitting the result as a function of the quark mass, we obtain γ_F^* to the statistical accuracy of 1 % level for the whole quark mass region below the charm quark mass including the chiral limit.

Then we estimate the systematic uncertainties of γ_F^* which are mainly due to $O(\alpha a)$ and $O(a^2)$ lattice artifacts. We also investigate how these systematic errors as well as the statistical error affect the meson masses, in the region $m_s < m_q < m_c$. The response of hadron masses with respect to γ_F in the light quark mass region, $m_q < m_s$, needs additional care, and is the subject of next section. At the end of this section, we summarize the result of calibration.

4.1 Simulation Parameters for the Calibration

In this work, we use three lattices with $\beta = 5.75, 5.95$ and 6.10 and the renormalized anisotropy $\xi = 4$. The value of γ_G corresponding to the desired value of ξ has been studied in detail by Klassen [5], and we can use his relation of γ_G and ξ which is obtained in one percent accuracy. The statistical uncertainties are, otherwise noted, estimated by the single elimination Jackknife method with appropriate binning. The configurations are separated by 2000 (1000) pseudo-heat-bath sweeps, after 20000 (10000) thermalization sweeps at $\beta=5.95$ and 6.10 (5.75). The configurations are fixed to the Coulomb gauge, which is particularly useful for the smearing of hadron operators.

The lattice cutoffs and the mean-field values of link variables are determined on the smaller lattices with half size in temporal extent for $\beta = 5.75, 5.95$, and otherwise with the same parameters, while at $\beta = 6.10$ the lattice size is $16^3 \times 64$. To obtain the lattice cutoffs, the static quark potential is measured with standard procedure. We adopt the hadronic radius r_0 proposed by Sommer [14] to set the scale. Following the method in Ref. [14], we determine the force between static quark and antiquark, as a function of r_I , the interquark distance improved with the lattice one-gluon exchange potential form. Then we fit the values of force, containing the off-axis data, to the form $\sigma + A/r_I^2$ in the fitting region roughly $0.5r_0 < r_I < 2r_0$. The parameters σ and A would be identified as the string tension and the Coulomb coefficient. The systematic uncertainty due to the choice of fit range is small, and at most the same size as the

Table 1: Lattice parameters. The scale a_σ^{-1} is determined from the hadronic radius r_0 . The mean-field values are in the Landau gauge. The statistical uncertainty of u_τ is less than the last digit.

β	γ_G	size	r_0	a_σ^{-1} [GeV]	u_σ	u_τ	η_{MF}
5.75	3.072	$12^3 \times 96$	2.786(15)	1.100(6)	0.7620(2)	0.9871	1.2953(4)
5.95	3.1586	$16^3 \times 128$	4.110(23)	1.623(9)	0.7917(1)	0.9891	1.2494(2)
6.10	3.2108	$20^3 \times 160$	5.140(32)	2.030(13)	0.8059(1)	0.9901	1.2285(2)

statistical error. Table 1 shows the value of r_0 and the a_σ^{-1} determined by setting the physical value of r_0 as $r_0^{-1} = 395$ MeV ($r_0 \simeq 0.5$ fm). The quoted error represent only the statistical uncertainty.

The mean-field values, u_σ and u_τ , are obtained as the average of the link variables in the Landau gauge, where the mean-field values are used self-consistently in the fixing condition [6]. The results are also listed in Table 1. The mean-field value of the temporal gauge field has small error, and close to unity. $\eta_{MF} = u_\tau/u_\sigma$, the mean-field estimate of $\eta = \xi/\gamma_G$, is close to the value of η determined nonperturbatively by Klassen. This suggest that the tadpole-improvement works well also on the anisotropic lattice.

4.2 Quark field calibration

As described in Section 3, we use the relativistic dispersion relation in the calibration of parameters in the quark action. Since the gauge field calibration is in the accuracy of one percent, we aim to tune the quark parameters to a similar level.

For convenience, we choose κ and γ_F as the input parameters and determine κ_σ and κ_τ along eq. (2.5). Fixing κ corresponds to fixing the bare quark mass in the spatial lattice unit. For each values of (κ, γ_F) , the pseudoscalar and vector meson correlators are obtained with zero and finite momenta. The fermionic anisotropy ξ_F is defined through the relativistic dispersion relation, eq. (3.2). We assume the linear dependence of ξ_F on γ_F in the vicinity of $\xi_F \simeq \xi$. We use linear interpolation to obtain γ_F^* , the value of γ_F with which the relation $\xi_F = \xi$ holds.

Result of the dispersion relation. The parameters (κ, γ_F) used in the calibration are listed in Table 2, 3 and 4 for $\beta = 5.75, 5.95$ and 6.10 , respectively. As the meson operators at the source, we adopt the smeared operators with appropriate smearing functions. For the light quark region, the Gaussian function is used as the smearing function, with the width of $0.2 \sim 0.4$ fm. In the charm quark mass region, we also use the measured wave function for the smearing function. We measure the two point functions for momenta $\mathbf{p} = \mathbf{n} \cdot (2\pi/L)$, where L is spatial lattice extent and $\mathbf{n} = (0, 0, 0), (1, 0, 0), (1, 1, 0), (1, 1, 1)$ and $(2, 0, 0)$. All rotationally equivalent \mathbf{n} 's are averaged. The standard procedure is used in extracting the energy at each momentum.

The energies are then fitted to the linear or quadratic forms in \mathbf{p}^2 to extract the fermionic anisotropy ξ_F in each channel. In the case of linear fit, we use only three lowest momentum states, $\mathbf{n} = (0, 0, 0), (1, 0, 0)$ and $(1, 1, 0)$. We assume the linear dependence of $\xi_F(\gamma_F)$ in γ_F , and this is indeed verified in several examples.

Figure 2 shows typical effective mass plots for pseudoscalar and the vector mesons. The energies of finite momentum states are successfully extracted from the region in which the correlator shows plateaus except the lightest quark region, $\kappa \leq 0.120$, which severely suffer

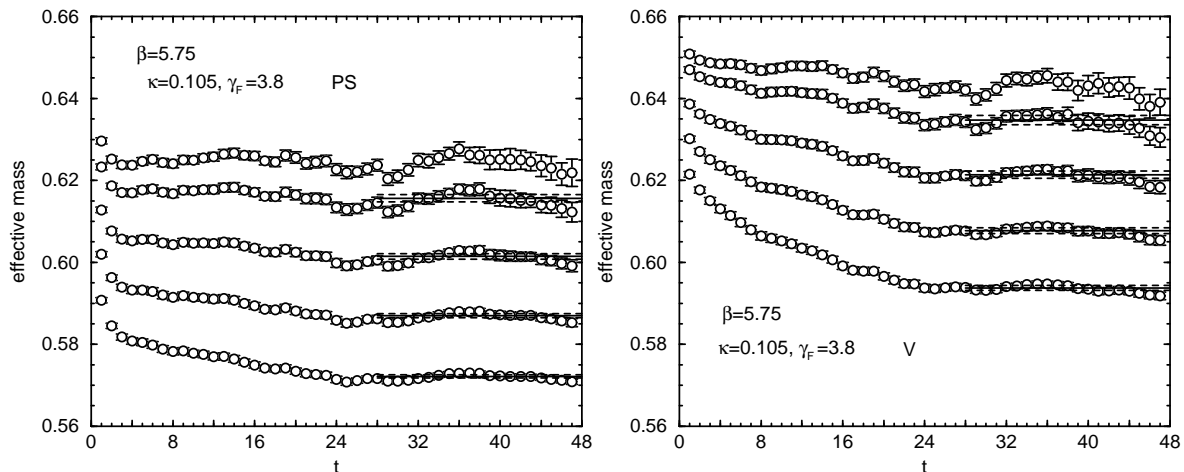


Figure 2: Effective mass plots of PS and V mesons at $\kappa = 0.105$, $\gamma_F = 3.8$ on $\beta = 5.75$ lattice. From bottom to top, the states with integer momentum vectors $\mathbf{n} = (0, 0, 0)$, $(1, 0, 0)$, $(1, 1, 0)$, $(1, 1, 1)$ and $(2, 0, 0)$. Horizontal solid lines represent the result of fit of correlators and the fitting range. The statistical errors are represented by the dashed lines. The state with $\mathbf{n} = (2, 0, 0)$ state is not used in the fit of the dispersion relation at this β .

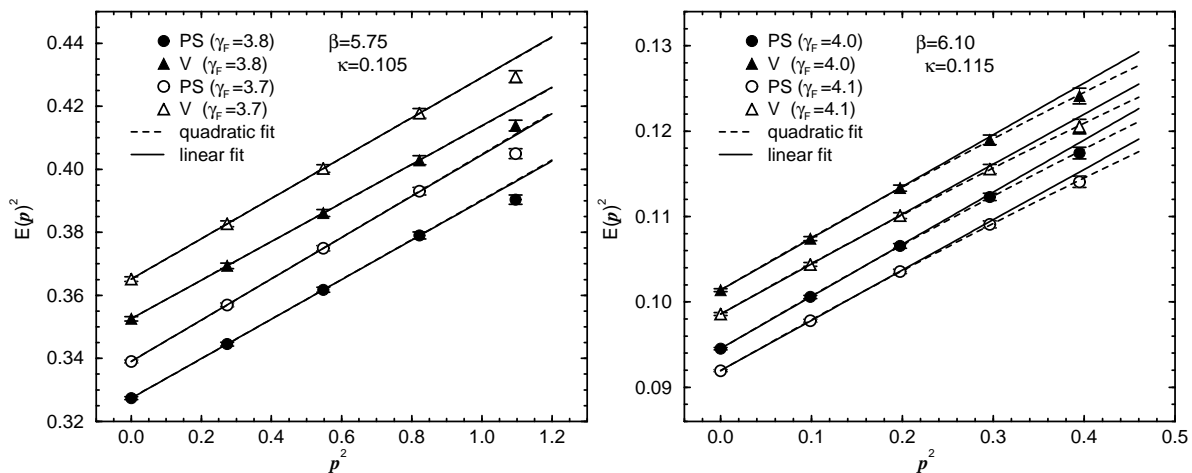


Figure 3: Dispersion relations of PS and V mesons. The left figure shows the data at $\kappa = 0.105$, $\gamma_F = 3.8$ and 3.7 on $\beta = 5.75$ lattice. The right figure shows those at $\kappa = 0.115$, $\gamma_F = 4.0$ and 4.1 on $\beta = 6.10$ lattice. Solid lines represent the linear fit and the dashed lines show the quadratic fit.

from the statistical fluctuation.

The dispersion relation for $\kappa = 0.105$ at $\beta = 5.75$ is shown in the left figure of Figure 3. Because of rather large lattice artifact, the fit to the quadratic form in \mathbf{p}^2 with the energy of $\mathbf{n} = (2, 0, 0)$ state is not a good description of data. We therefore use only four lowest energy states in the quadratic fit. On the other hand, the results of the linear fit (with lowest three states) and the quadratic fit coincides with good accuracy. For a few largest hopping parameters, higher momentum states suffers so large statistical fluctuations that we inevitably

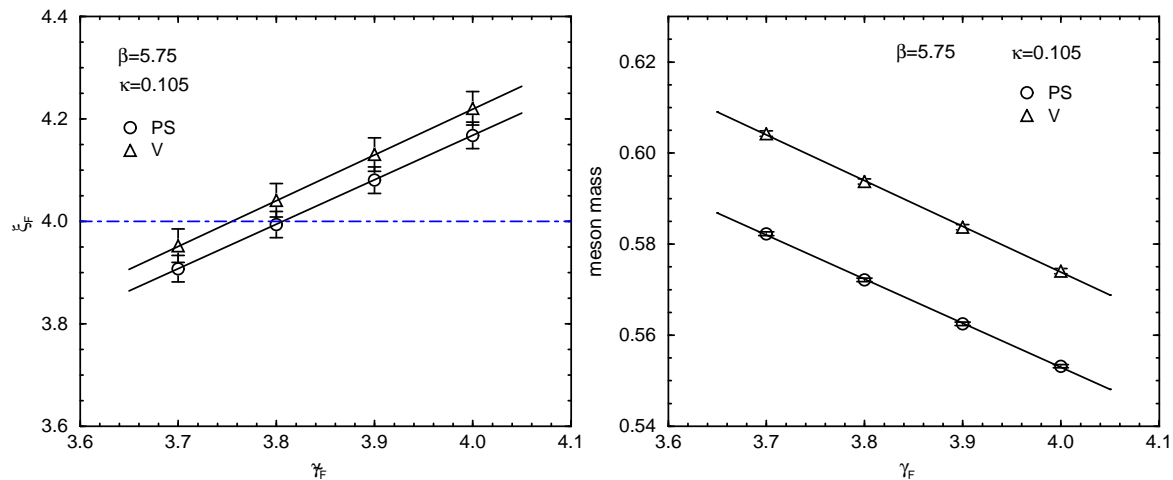


Figure 4: γ_F dependence of ξ_F (left) and meson masses (right) at $\kappa = 0.105$ on $\beta = 5.75$ lattice.

adopt the linear fit. Since at other values of κ the resultant ξ_F coincides with quadratic fit, we adopt the linear fit for all values of κ at this β . Since the same method as $\beta = 5.75$ case is adopted at $\beta = 5.95$, we do not repeat the explanation for the fitting procedure.

The right figure of Figure 3 shows the dispersion relation of mesons at $\beta = 6.10$ and $\kappa = 0.115$, which corresponds to a similar quark mass as $\kappa = 0.105$ at $\beta = 5.75$. The dispersion relation is much improved, and the quadratic fit is successfully applied including $\mathbf{n} = (2, 0, 0)$ state. Although the difference between the linear fit is small, as is shown in the figure, we adopt the result of quadratic fit to determine ξ_F except for most light quark region. For these three largest κ , correlators with $\mathbf{n} = (2, 0, 0)$, and occasionally $(1, 1, 1)$, suffer from so large statistical fluctuations that the energy of the states cannot be reliably extracted. In these cases, we fit the energy to the linear form.

Calibration of γ_F for each quark mass. In the left figure of Figure 4, ξ_F is plotted as the function of γ_F for $\kappa = 0.105$ at $\beta = 5.75$. It is clear that ξ_F depends linearly on γ_F . The results at $\kappa = 0.101, 0.110$ and 0.112 also show similar behavior. We therefore assume the linear dependence also for other values of κ , and interpolate ξ_F to find out γ_F^* in each channel. The numerical results of $\gamma_F^{*(PS)}$, $\gamma_F^{*(V)}$ and γ_F^* as the average over PS and V mesons are listed in Table 2–4 for each β . These tables also show the interpolated masses of PS and V mesons. We find a tendency that $\gamma_F^{*(PS)}$ is slightly larger than $\gamma_F^{*(V)}$ in whole κ region. This deviation seems to become smaller for larger β . The reason for the discrepancy is understood as the systematic errors of $O(\alpha a)$, which will be examined in the next subsection in detail.

We also plot the γ_F dependence of meson masses at $\kappa = 0.105$ and $\beta = 5.75$ in the right figure of Figure 4. This shows that the meson mass is linear in γ_F in this range, and linear interpolation is successfully applicable to determine the meson masses at γ_F^* . Although the γ_F dependence of meson mass is in general unknown for other region of κ , we expect that the linear interpolation would work in good accuracy. The meson masses at γ_F^* are also listed in Table 2–4 for each β . How the uncertainty in γ_F^* affect on the spectrum is an important problem, which will be examined in the next subsection.

Table 2: Calibration parameters and result at $\beta = 5.75$. Linear fit is applied to the dispersion relation in the determination of ξ_F .

κ	input γ_F	N_{conf}	$\gamma_F^{*(PS)}$	$\gamma_F^{*(V)}$	γ_F^*	$m_{PS}(\gamma_F^*)$	$m_V(\gamma_F^*)$
0.124	3.9, 4.0	400	3.935(77)	3.83(18)	3.919(72)	0.1497(6)	0.2294(17)
0.122	3.9, 4.0	400	3.904(48)	3.884(82)	3.899(45)	0.2044(4)	0.2650(12)
0.120	3.9, 4.0	400	3.892(43)	3.888(54)	3.891(38)	0.2523(8)	0.3018(12)
0.118	3.9, 4.0	400	3.906(36)	3.894(42)	3.901(31)	0.2967(9)	0.3387(12)
0.116	3.9, 4.0	300	3.875(35)	3.841(42)	3.861(33)	0.3408(13)	0.3774(15)
0.114	3.9, 4.0	200	3.899(36)	3.842(47)	3.878(36)	0.3819(17)	0.4142(19)
0.112	3.8, 3.9, 4.0	200	3.854(29)	3.806(37)	3.836(30)	0.4252(17)	0.4546(18)
0.110	3.8, 3.9, 4.0	200	3.878(33)	3.827(41)	3.857(34)	0.4654(22)	0.4918(23)
0.105	3.7, 3.8, 3.9, 4.0	160	3.807(30)	3.754(37)	3.786(31)	0.5738(28)	0.5954(28)
0.101	3.7, 3.8, 3.9, 4.0	160	3.730(26)	3.679(31)	3.709(27)	0.6653(30)	0.6845(30)
0.097	3.5, 3.6	160	3.626(19)	3.587(24)	3.611(20)	0.7647(28)	0.7823(28)
0.095	3.5, 3.6	160	3.579(18)	3.540(23)	3.564(19)	0.8166(29)	0.8333(29)
0.093	3.5, 3.6	160	3.530(17)	3.490(21)	3.514(18)	0.8704(29)	0.8864(29)

Table 3: Calibration parameters and result at $\beta = 5.95$. Linear fit is applied to the dispersion relation in the determination of ξ_F .

κ	input γ_F	N_{conf}	$\gamma_F^{*(PS)}$	$\gamma_F^{*(V)}$	γ_F^*	$m_{PS}(\gamma_F^*)$	$m_V(\gamma_F^*)$
0.124	3.9, 4.0	500	4.073(95)	4.15(12)	4.103(80)	0.1177(6)	0.1649(9)
0.123	3.9, 4.0	500	4.041(69)	4.095(93)	4.060(60)	0.1456(2)	0.1847(8)
0.122	3.9, 4.0	500	4.029(55)	4.076(68)	4.048(48)	0.1712(4)	0.2045(8)
0.120	3.9, 4.0	500	4.019(36)	3.996(55)	4.012(34)	0.2186(6)	0.2444(9)
0.118	3.9, 4.0	500	4.003(29)	4.000(35)	4.002(28)	0.2625(8)	0.2841(9)
0.115	3.9, 4.0	360	3.992(28)	3.969(36)	3.983(29)	0.3260(12)	0.3431(13)
0.110	3.9, 4.0	300	3.945(28)	3.946(36)	3.946(29)	0.4297(19)	0.4427(19)
0.107	3.9, 4.0	300	3.910(25)	3.911(31)	3.910(26)	0.4930(20)	0.5046(21)
0.104	3.9, 4.0	200	3.876(28)	3.875(36)	3.876(30)	0.5573(27)	0.5677(27)
0.102	3.9, 4.0	200	3.848(26)	3.847(34)	3.847(28)	0.6016(28)	0.6113(28)
0.100	3.9, 4.0	200	3.815(25)	3.816(32)	3.815(27)	0.6470(29)	0.6562(29)
0.097	3.8, 3.9	200	3.766(24)	3.765(30)	3.766(26)	0.7178(32)	0.7264(32)
0.093	3.7, 3.8	200	3.688(23)	3.687(29)	3.688(25)	0.8180(37)	0.8257(37)

Fit of γ_F^* . To represent γ_F^* as the function of κ , we introduce the quark mass as

$$m_q = \frac{1}{2\xi} \left(\frac{1}{\kappa} - \frac{1}{\kappa_c} \right). \quad (4.1)$$

This is similar relation as m_0 , the bare quark mass in the temporal lattice unit, while the present form is independent of γ_F . κ_c is determined from massless point of the pseudoscalar meson mass. We extrapolate m_{PS}^2 linearly in $1/\kappa$ using two largest values of κ , and find as $\kappa_c = 0.12640(5)$ at $\beta = 5.75$, $0.12592(6)$ at $\beta = 5.95$ and $0.12558(4)$ at $\beta = 6.10$.

In the calibration at each κ , we found that the value of γ_F^* is easily determined precisely (to the level of 1 %), while it become difficult with increasing κ toward κ_c . However, it is expected

Table 4: Calibration parameters and result at $\beta = 6.10$. For $\kappa = 0.124, 0.123$ and 0.122 , the dispersion relation is fitted to the linear form in determining ξ_F . For the remaining κ 's, quadratic fit is applied.

κ	input γ_F	N_{conf}	$\gamma_F^{*(PS)}$	$\gamma_F^{*(V)}$	γ_F^*	$m_{PS}(\gamma_F^*)$	$m_V(\gamma_F^*)$
0.124	4.0, 4.1	600	4.020(77)	3.63(27)	3.991(79)	0.1008(5)	0.1379(7)
0.123	4.0, 4.1	600	4.005(52)	3.860(98)	3.973(55)	0.1294(1)	0.1582(5)
0.122	4.0, 4.1	600	3.998(41)	3.913(69)	3.976(44)	0.1549(3)	0.1787(6)
0.120	4.0, 4.1	400	4.040(29)	4.064(45)	4.047(30)	0.2007(6)	0.2182(7)
0.118	4.0, 4.1	200	4.040(33)	4.014(52)	4.032(34)	0.2440(9)	0.2579(10)
0.115	4.0, 4.1	200	4.024(28)	4.008(41)	4.019(30)	0.3067(12)	0.3176(13)
0.110	4.0, 4.1	200	4.013(38)	3.996(54)	4.007(43)	0.4078(26)	0.4160(27)
0.107	4.0, 4.1	200	3.988(36)	3.986(46)	3.987(39)	0.4694(29)	0.4766(30)
0.104	4.0, 4.1	200	3.951(33)	3.955(42)	3.952(36)	0.5331(31)	0.5396(31)
0.102	3.9, 4.0	200	3.918(32)	3.928(40)	3.922(35)	0.5773(34)	0.5834(34)
0.100	3.9, 4.0	200	3.877(25)	3.883(32)	3.879(27)	0.6240(28)	0.6298(28)
0.097	3.9, 4.0	200	3.834(22)	3.839(28)	3.836(24)	0.6931(28)	0.6984(28)
0.093	3.8, 3.9	200	3.769(21)	3.776(26)	3.772(23)	0.7903(32)	0.7953(31)

γ_F^* smoothly approaches to certain definite value in the limit of $m_q \rightarrow 0$, since in this limit our form of action is simply a direct generalization of clover quark action on the anisotropic lattice. In fact, as shown in Subsection 2.2, γ_F^* linearly depends on m_0^2 at the tree level. In taking the limit of $m_q \rightarrow 0$ for γ_F^* , the precise values of mean-field values do not matter, since in the definition of γ_F , tadpole-improvement is applied as a multiplicative factor, $\eta_{MF} = u_\tau/u_\sigma$. Therefore the most reliable way to determine the value of γ_F^* in the light quark region is a global fit of γ_F^* , assuming appropriate form of m_q dependence.

We fit the result of $1/\gamma_F^*$ to the linear form in m_q^2 and the quadratic form in m_q . The result of fit is listed in Table 5 and also shown in Figures 5 as the solid and the dashed curves. Since the obtained points for γ_F^* is with different number of configurations, these points correlate in not obvious way. We quote the errors and χ^2 of uncorrelated fit in Table 5. As shown in these table and figures, the linear fit in m_q^2 well represents the data. The values of ζ_0 , which is the $1/\gamma_F^*$ in the chiral limit, is close to the tree level result $1/\xi = 1/4$, which implies that the tadpole-improvement works well. Apart from the lightest quark mass region, γ_F^* is determined within 1 % accuracy, and there the curves of two fits are consistent with each other. In approaching the chiral limit, there is a systematic error concerning the fit form, as well as the statistical error. We estimate the latter by the error of fit in ζ_0 (from the quadratic fit in m_q^2), and as about 1 %. This relatively small statistical error is due to the global fit of $1/\gamma_F^*$ with assumed form of m_q dependence. The systematic error in adopting specific form of fit is estimated by the difference between these two fits, and also results in 1 % level. Adopting the linear form in m_q^2 , we conclude that the γ_F^* is determined under the assumed dispersion relation within 1 % statistical accuracy in the whole quark mass region less than around the charm quark mass, while in the chiral limit there is additional 1 % systematic uncertainty concerning the form of fit.

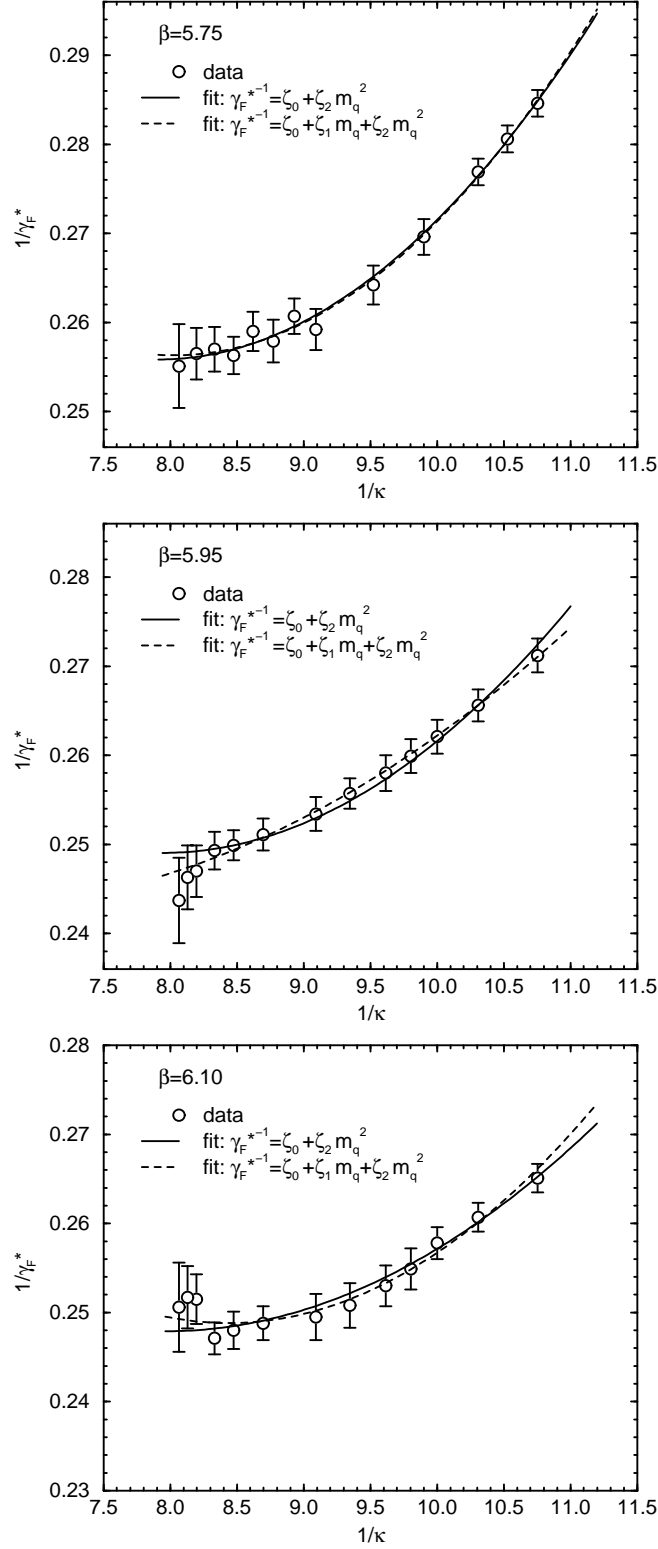


Figure 5: $1/\gamma_F^*$ vs $1/\kappa$ at each β . Solid lines show the fit linear in m_q^2 while the dashed lines represent the fit quadratic in m_q .

Table 5: Fit results of γ_F .

β	fit type	ζ_0	ζ_1	ζ_2	χ^2/N_{df}	$\gamma_F^*(m_q = 0)$
5.75	linear	0.2558(9)	–	0.230(12)	1.83 / 11	3.909(14)
	quad.	0.2564(23)	–0.007(28)	0.247(68)	1.77 / 10	3.901(34)
5.95	linear	0.2490(8)	–	0.189(15)	3.52 / 11	4.016(13)
	quad.	0.2465(18)	0.036(23)	0.095(61)	1.01 / 10	4.057(30)
6.10	linear	0.2479(9)	–	0.143(14)	4.44 / 11	4.034(14)
	quad.	0.2493(18)	–0.022(24)	0.200(63)	3.55 / 10	4.011(28)

4.3 Uncertainties in calibration

In the last subsection, we determined γ_F^* as a global function of m_q . This expression inevitably suffer from systematic uncertainties as well as the statistical uncertainty:

$$\gamma_F^* = \gamma_F^{*(prop)} + \delta\gamma_F^{(stat)} + \delta\gamma_F^{(O(\alpha a))} + \delta\gamma_F^{(O(a^2))} (+\delta\gamma_F^{(chiral)}). \quad (4.2)$$

$\gamma_F^{*(prop)}$ represent the proper value of the bare anisotropy. $\delta\gamma_F^{(stat)}$ is the statistical error in determination of γ_F^* , and at 1 % level. The last two terms are main sources of systematic errors due to finite lattice artifact. The first one, $\delta\gamma_F^{(O(\alpha a))}$, is from the tree-level approximation of clover coefficients. We estimate the size of this error by the difference between the values of γ_F^* determined with PS and V mesons. The second systematic error, $\delta\gamma_F^{(O(a^2))}$, is estimated by comparing the results of calibration from two different forms of dispersion relations which differ by $O(a^2)$. In addition to these systematic uncertainties, in the chiral limit there is also a systematic error concerning the form of fit of γ_F^* in m_q .

Another important subject is to estimate how the observables are affected by the uncertainty in γ_F^* . We study the response of meson masses with respect to the change of γ_F^* at each κ , from which the effect of γ_F on meson masses for given quark mass is approximately estimated. Strictly speaking, changing γ_F for a fixed κ induces a slight change in the quark mass, hence the above analysis is adequate for relatively heavier quark mass region, such as $m_s < m_q$. We postpone the study of the effect on the light hadron spectrum to the end of next section.

Difference between $\gamma_F^{*(PS)}$ and $\gamma_F^{*(V)}$. Since we use the $O(a)$ improved quark action, the main contribution from the $O(a)$ lattice artifact is absent. However, since the clover coefficients are not tuned beyond the tree-level, $O(\alpha a)$ error still remains, although the tadpole-improvement would partially removes this effect. An appropriate probe of this systematic effect on the calibration is the difference between γ_F^* 's of the pseudoscalar and the vector mesons. Figure 6 shows $\delta\gamma_F^* \equiv \gamma_F^{*(PS)} - \gamma_F^{*(V)}$. At $\beta = 5.75$, there is a systematic difference of $\delta\gamma_F^*$ from zero except the small quark mass region, where the statistical error is dominant. At $\beta = 5.95$, $\delta\gamma_F^*$ is consistent with zero in whole κ region. This implies that the $O(\alpha a)$ error in the calibration is sufficiently reduced at this β . In the case of $\beta = 6.10$, $\delta\gamma_F^*$ is also consistent with zero except the lightest quark region. In this region, precise determination of energy at finite momentum states is difficult due to the statistical fluctuation and hence the resultant γ_F contains large uncertainty. We regard that the $O(\alpha a)$ effect in the calibration is also small at this β .

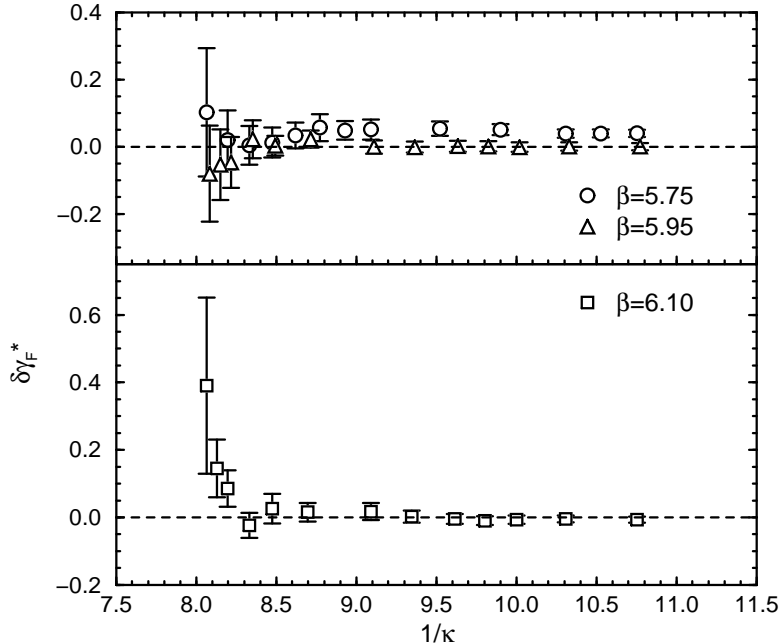


Figure 6: $\delta\gamma_F^* = \gamma_F^{*(PS)} - \gamma_F^{*(V)}$ at $\beta = 5.75$ and 5.95 in upper part, and 6.10 in lower part.

$O(a^2)$ systematic uncertainty. Although we employed the continuum dispersion relation, this introduces a systematic error of $O(a^2)$ to the calibration of γ_F . In order to estimate the typical size of this error, we compare γ_F^* determined above with $\gamma_{F(KG)}^*$, the result obtained using the dispersion relation from the lattice Klein-Gordon action, (3.3). Figure 7 shows this comparison at $\beta = 5.75$ and 6.10 . In extracting ξ_{KG} from the Klein-Gordon dispersion relation, we fit $\cosh E(\mathbf{p})$ to the linear form in $\sum_i \sin^2(p_i/2)$ using lowest three momentum states. As explained in Section 3, expected difference of ξ_F and ξ_{KG} is $O(m^2)$, where m is the meson mass. Although the explicit relation between $\gamma_{F(KG)}^*$ and γ_F^* is unknown, one can expect that the difference of them is also in $O(m^2)$, and hence increase with increasing quark mass. This behavior is clearly observed in Figure 7. Table 6 is the result of fit of $\gamma_{F(KG)}^*$ to the linear form in m_q^2 .

We find small difference between the results with relativistic and Klein-Gordon dispersion relations in the small quark mass region. This difference decreases as increasing β , and seems to be sufficiently reduced at $\beta = 6.10$. The typical size of difference in γ_F^* 's at the chiral limit is less than 3, 2, 1 % at $\beta = 5.75, 5.95$ and 6.10 , respectively. The important feature is that two procedures tend to coincide with each other with increasing β . We also observe that the difference between γ_F^* and $\gamma_{F(KG)}^*$ increases in the large quark mass region, $m_q > 0.2a_\tau^{-1}$. This is consistent behavior, since there the Klein-Gordon dispersion relation fails to incorporate the quark mass dependence properly, and $\gamma_{F(KG)}^*$ is expected to be larger than γ_F^* in $O(m^2)$. Therefore we conclude that the uncertainty due to the assumed form of the meson dispersion relation is under control and smoothly disappears in approaching the continuum limit.

Uncertainty in meson mass due to calibration error. Another important issue on the systematic errors is how the uncertainty in γ_F is transmitted to the observables. As an important example, here we focus on the effect on the meson masses.

Since we linearly interpolate the meson masses in γ_F , we obtain $dm/d\gamma_F$ at $\gamma_F = \gamma_F^*$ from

Table 6: The result of linear fit in m_q^2 of $\gamma_{F(KG)}^*$, the tuned bare anisotropy with the Klein-Gordon dispersion relation.

β	fit type	ζ_0	ζ_2	χ^2/N_{df}	$\gamma_F^*(m_q = 0)$
5.75	linear	0.2488(8)	0.112(11)	2.33 / 11	4.019(13)
5.95	linear	0.2446(8)	0.071(14)	2.14 / 11	4.088(13)
6.10	linear	0.2484(10)	0.039(15)	1.59 / 11	4.026(16)

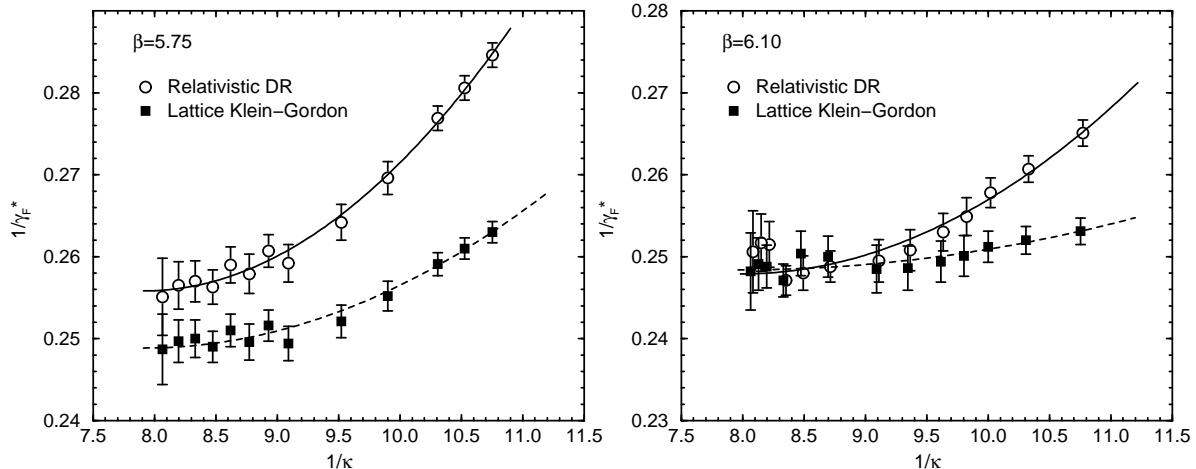


Figure 7: Comparison of the results of calibrations with two types of dispersion relations. The curves represent the the result of linear fit in m_0^2 . Solid lines are the fit results with relativistic dispersion relation and the dashed lines are those with Lattice Klein-Gordon dispersion relation.

the slope of the linear fit. In Figure 8, we show $dm/d\gamma_F$, the response of meson mass to the bare anisotropy, at $\beta = 6.10$ in two ways. Similar feature is found in the results at $\beta = 5.75$ and $\beta = 5.95$. In the left figure $dm/d\gamma_F$ is shown as the function of $1/\kappa$. In the case of vector meson, it seems to decrease linearly in quark mass from zero at the massless limit. On the other hand, for the pseudoscalar meson, $dm/d\gamma_F$ slightly positive in the vicinity of $1/\kappa_c$. This behavior may be due to the uncertainty in the definition of κ , because if κ is properly related to the fixed quark mass, increasing γ_F implies to increase the propagation in temporal direction, hence it corresponds to decreasing quark mass. Therefore, the present analysis may not be adequate for estimating the response of masses with respect to γ_F in the vicinity of the chiral limit. Observing Figure 8, one can find that the range of quark mass larger than the strange quark mass do not suffer from the ambiguity in the definition of κ .

We have no clear explanation for that $dm/d\gamma_F$ seems to be proportional to the quark mass. Practically, it is a good feature that the ambiguity of γ_F^* has only little effects on the meson mass in the small but nonzero quark mass region, since there relative change of mass is significant. Except the lightest quark mass region, the determination of γ_F^* is directly performed with 1 % accuracy, which means the uncertainty of γ_F^* is around 0.04. The right figure in Figure 8 implies that the uncertainty in the meson mass is less than 1 %. This uncertainty is most severe in the heavy quark region, and become milder as quark mass decreases.

While we find that the meson masses at certain κ is not so sensitive to the uncertainty of γ_F^* , the same argument does not hold for the chiral limit. Since the pseudoscalar meson

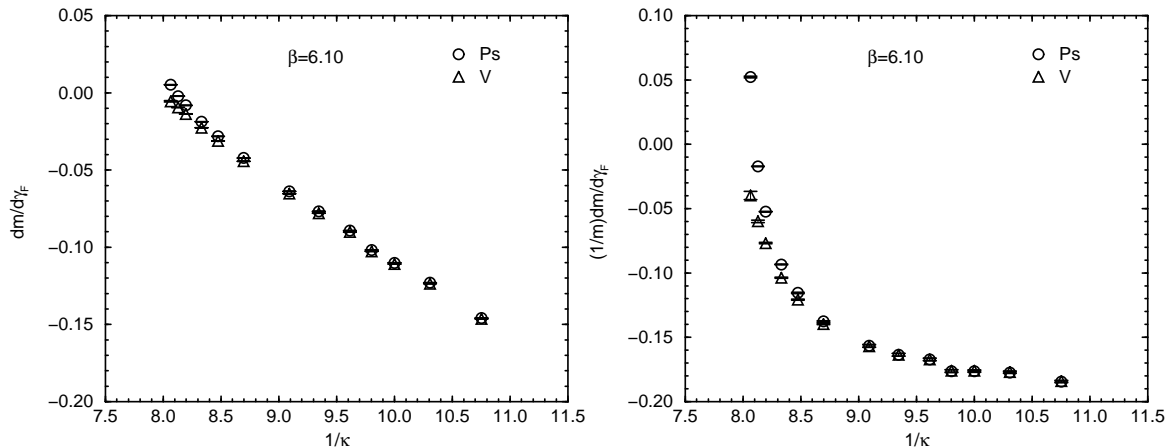


Figure 8: The response of meson masses to the change of γ_F at $\beta = 6.10$. The left figure shows $dm/d\gamma_F$, while the ratio $(1/m)dm/d\gamma_F$ is shown in the right figure. The result for the pseudoscalar and the vector mesons are represented by circles and triangles respectively.

mass becomes zero in the chiral limit, the relative uncertainties $\delta m_{PS}/m_{PS}$ for a fixed κ near the chiral limit is of course very large. However, this is not the correct way to estimate the uncertainties in the mass spectrum in the chiral limit. What one is really interested in for the chiral limit is not the change the hadron masses including the pion mass for a fixed κ but the change of hadron masses except the pion mass at the point where the pion becomes massless. Since the critical hopping parameter κ_c is affected by the change in γ_F , one need to treat the chiral limit carefully. In the next section, we discuss the uncertainties of the hadron spectrum in the chiral limit based on the extrapolation in terms of the pseudoscalar meson mass squared instead of $1/\kappa$.

4.4 Summary of calibration

In this section, we have implemented the anisotropic $O(a)$ improved Wilson action in the region of quark mass up to around the charm quark mass, at three values of β at $\xi = 4.0$. The fermionic anisotropy ξ_F is extracted from the meson dispersion relation. Then we find the value of bare anisotropy parameter, γ_F^* , at which $\xi_F = \xi$ holds. The value of γ_F^* in the massless limit is obtained by extrapolating the data by fitting to the linear form in m_q^2 , where m_q is naively defined quark mass. This is the most reliable way to determine γ_F^* for small quark mass region, since there the statistical fluctuation in finite momentum states is severely large. The fit of $1/\gamma_F^*$ to the linear form in m_q^2 seems quite successful, and γ_F^* at the chiral limit is close to the tree-level value, ξ . The statistical uncertainty in γ_F^* is estimated as in the order of 1 % in whole explored quark mass region. In the chiral limit, there is also 1 % systematic uncertainty concerning the form of fit. Here we summarize the main result of calibration, the expression of γ_F^* for a given κ :

$$\frac{1}{\gamma_F^*}(m_q) = \zeta_0 + \zeta_2 m_q^2, \quad m_q = \frac{1}{2\xi} \left(\frac{1}{\kappa} - \frac{1}{\kappa_c} \right), \quad (4.3)$$

$$\beta = 5.75 : \quad \zeta_0 = 0.2558(9), \quad \zeta_2 = 0.230(12), \quad \kappa_c = 0.12640(5) \quad (4.4)$$

$$\beta = 5.95 : \quad \zeta_0 = 0.2490(8), \quad \zeta_2 = 0.189(15), \quad \kappa_c = 0.12592(6) \quad (4.5)$$

$$\beta = 6.10 : \quad \zeta_0 = 0.2479(9), \quad \zeta_2 = 0.143(14), \quad \kappa_c = 0.12558(4). \quad (4.6)$$

Table 7: Quark parameters used in the hadron spectroscopy.

β	γ_F	values of κ	N_{conf}
5.75	3.909	0.1240, 0.1230, 0.1220, 0.1210	200
5.95	4.016	0.1245, 0.1240, 0.1235, 0.1230	100
6.10	4.034	0.1245, 0.1240, 0.1235, 0.1230	100

To examine the uncertainty in the calibration, we have also carried out the following analysis. (i). The difference between γ_F^* for the pseudoscalar and vector mesons, which signals the $O(a)$ systematic error. We observed that this difference decreases as decreasing lattice spacing, and already consistent with zero at $\beta = 5.95$. (ii). Comparison of γ_F^* with the continuum and the Klein-Gordon dispersion relations. This is for an estimate of the size of $O(a^2)$ systematic uncertainty. The results with two dispersion relations tends to coincide with each other in decreasing the lattice spacing. The behavior in the large quark mass region is consistent with the expected behavior. (iii). Response of meson masses to the change of γ_F . The effect of uncertainty of γ_F^* on the meson masses is less than 1 %, if γ_F^* is determined at this accuracy. This result is applicable to the relatively heavier quark mass region, such as $m_s < m_q$, and therefore in the region, the errors in the calibration is under control.

5 Light hadron spectroscopy

In this section, we apply the result of the last section to the calculation of light hadron spectrum. Our analysis is performed in two steps:

(i) By taking the central value of $\gamma_F = \gamma_F^*$ we obtain the light hadron masses in the strange quark mass region $m_s < m_q < 2m_s$. By extrapolating masses in m_{PS}^2 , the hadron spectrum at the physical light quark masses are determined. We compare our result with the result by UKQCD Collaboration [15], which has been obtained on the isotropic lattice with $O(a)$ improved quark action.

(ii) We study the response of the light hadron spectrum to the change of the anisotropic parameter $\gamma_F^* \rightarrow \gamma_F^* + \delta\gamma_F$. The extrapolation in m_{PS}^2 is significant to circumvent the uncertainty in the definition of κ .

5.1 Calculation of hadron spectrum

The spectroscopy of light hadrons are performed on the same lattices used in the calibration, while with smaller numbers of configurations. The parameters are listed in Table 7. At each β , we use four values of κ corresponding to the quark mass of m_s-2m_s . In this region, we regard that m_q is sufficiently small so that we can adopt the value of γ_F^* in the massless limit. Therefore the bare anisotropy is set to the central value of γ_F^* at $m_q = 0$, which is determined in the calibration as the linear form in m_q^2 .

We use the standard hadron operators and procedure to extract the hadron masses. The quark propagators are smeared at the source with Gaussian smearing function with the deviation $\simeq 0.4$ fm, in the Coulomb gauge. The periodic boundary condition is adopted in all four directions for the quark field. For baryons, two of quarks are treated as they have degenerate masses. Then the quark content of baryons is specified by two κ 's, κ_1 and κ_2 , for a pair of quarks and the other quark, respectively. Figure 9 shows the effective mass plot for octet and

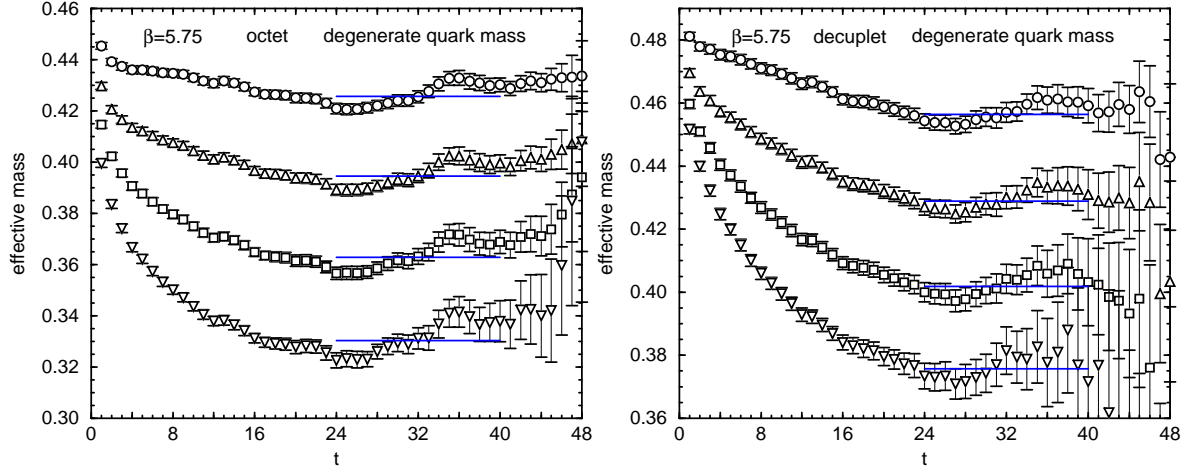


Figure 9: Effective mass plots for octet and decuplet baryon correlators with degenerate quark masses at $\beta = 5.75$. Horizontal solid line represent the fit range and the mass from the single exponential fit.

Table 8: Hadron spectrum at $\beta = 5.75$. When quark masses are degenerate, i.e. $\kappa_1 = \kappa_2$, the Σ -type and the Λ -type octet baryon correlators are identical.

κ_1	κ_2	m_{PS}	m_V	$m_{oct(\Sigma)}$	$m_{oct(\Lambda)}$	m_{dec}
0.1210	0.1210	0.22909(47)	0.2821(10)	0.4257(17)	–	0.4564(24)
0.1210	0.1220	0.21716(48)	0.2730(11)	0.4146(18)	0.4161(18)	0.4472(25)
0.1210	0.1230	0.20501(51)	0.2640(12)	0.4034(19)	0.4068(19)	0.4383(27)
0.1210	0.1240	0.19260(54)	0.2552(13)	0.3920(20)	0.3977(21)	0.4299(29)
0.1220	0.1210	–	–	0.4059(19)	0.4042(19)	0.4381(27)
0.1220	0.1220	0.20480(50)	0.2637(12)	0.3946(19)	–	0.4289(28)
0.1220	0.1230	0.19214(52)	0.2546(13)	0.3831(20)	0.3852(21)	0.4199(30)
0.1220	0.1240	0.17911(55)	0.2458(15)	0.3713(21)	0.3760(22)	0.4114(33)
0.1230	0.1210	–	–	0.3863(21)	0.3820(20)	0.4202(30)
0.1230	0.1220	–	–	0.3747(22)	0.3724(21)	0.4109(32)
0.1230	0.1230	0.17886(54)	0.2454(15)	0.3629(23)	–	0.4018(35)
0.1230	0.1240	0.16503(57)	0.2364(17)	0.3506(24)	0.3538(25)	0.3932(39)
0.1240	0.1210	–	–	0.3674(25)	0.3587(22)	0.4032(37)
0.1240	0.1220	–	–	0.3555(26)	0.3490(24)	0.3938(40)
0.1240	0.1230	–	–	0.3432(27)	0.3394(25)	0.3845(44)
0.1240	0.1240	0.15015(60)	0.2272(21)	0.3303(28)	–	0.3757(51)

decuplet baryons with degenerate quark mass case, $\kappa_1 = \kappa_2$. The meson correlators are fitted to the single hyperbolic cosine form. For baryons, we apply the single exponential fit in the region in which there is negligible contribution of the negative parity baryon from the other temporal boundary. The result of fit is listed in Tables 8– 10. For mesons, since the order of κ_1 and κ_2 is unimportant, the masses at the exchanged set of (κ_1, κ_2) are omitted. The masses of Λ -type octet baryon at degenerate (κ_1, κ_2) are also omitted, since they are identical to the masses of Σ -type.

Table 9: Hadron spectrum at $\beta = 5.85$.

κ_1	κ_2	m_{PS}	m_V	$m_{oct(\Sigma)}$	$m_{oct(\Lambda)}$	m_{dec}
0.1230	0.1230	0.14580(40)	0.1853(10)	0.2788(17)	–	0.3036(25)
0.1230	0.1235	0.13896(41)	0.1804(11)	0.2726(17)	0.2734(18)	0.2987(26)
0.1230	0.1240	0.13196(43)	0.1755(11)	0.2662(18)	0.2680(19)	0.2938(27)
0.1230	0.1245	0.12477(46)	0.1707(13)	0.2596(19)	0.2625(20)	0.2890(30)
0.1235	0.1230	–	–	0.2676(18)	0.2666(18)	0.2937(27)
0.1235	0.1235	0.13190(43)	0.1754(11)	0.2612(19)	–	0.2888(29)
0.1235	0.1240	0.12462(45)	0.1705(12)	0.2546(19)	0.2557(20)	0.2839(31)
0.1235	0.1245	0.11709(47)	0.1656(14)	0.2478(20)	0.2501(21)	0.2790(33)
0.1240	0.1230	–	–	0.2562(20)	0.2539(19)	0.2839(31)
0.1240	0.1235	–	–	0.2496(21)	0.2484(20)	0.2789(33)
0.1240	0.1240	0.11702(47)	0.1654(14)	0.2427(21)	–	0.2740(35)
0.1240	0.1245	0.10908(50)	0.1605(16)	0.2356(22)	0.2370(23)	0.2692(38)
0.1245	0.1230	–	–	0.2445(23)	0.2405(21)	0.2743(37)
0.1245	0.1235	–	–	0.2376(24)	0.2348(22)	0.2693(39)
0.1245	0.1240	–	–	0.2305(25)	0.2289(24)	0.2644(42)
0.1245	0.1245	0.10063(53)	0.1555(19)	0.2229(26)	–	0.2597(47)

Table 10: Hadron spectrum at $\beta = 6.10$.

κ_1	κ_2	m_{PS}	m_V	$m_{oct(\Sigma)}$	$m_{oct(\Lambda)}$	m_{dec}
0.1230	0.1230	0.12950(29)	0.1587(6)	0.2394(11)	–	0.2590(17)
0.1230	0.1235	0.12284(30)	0.1538(6)	0.2332(12)	0.2340(12)	0.2542(18)
0.1230	0.1240	0.11603(31)	0.1491(7)	0.2269(12)	0.2288(12)	0.2495(19)
0.1230	0.1245	0.10904(33)	0.1446(8)	0.2204(13)	0.2236(13)	0.2451(21)
0.1235	0.1230	–	–	0.2283(12)	0.2273(12)	0.2493(19)
0.1235	0.1235	0.11595(31)	0.1489(7)	0.2219(13)	–	0.2445(20)
0.1235	0.1240	0.10886(32)	0.1442(8)	0.2154(13)	0.2166(13)	0.2399(22)
0.1235	0.1245	0.10153(33)	0.1398(9)	0.2087(14)	0.2112(14)	0.2355(24)
0.1240	0.1230	–	–	0.2171(14)	0.2148(13)	0.2400(22)
0.1240	0.1235	–	–	0.2106(14)	0.2093(14)	0.2352(24)
0.1240	0.1240	0.10142(33)	0.1395(8)	0.2038(14)	–	0.2306(26)
0.1240	0.1245	0.09366(35)	0.1352(10)	0.1968(15)	0.1983(16)	0.2263(30)
0.1245	0.1230	–	–	0.2058(16)	0.2017(15)	0.2314(28)
0.1245	0.1235	–	–	0.1990(16)	0.1960(15)	0.2267(30)
0.1245	0.1240	–	–	0.1919(17)	0.1903(16)	0.2221(34)
0.1245	0.1245	0.08535(36)	0.1310(12)	0.1845(18)	–	0.2180(41)

5.2 Extrapolation to the chiral limit

In order to avoid the ambiguities in the definition of the quark mass, we extrapolate the hadron masses to the chiral limit in terms of the pseudoscalar meson mass squared, instead of $1/\kappa$.

We assume the relation

$$m_{PS}^2(m_1, m_2) = B \cdot (m_1 + m_2), \quad (5.1)$$

then for the degenerate quark masses, $m_1 = m_2$, $m_{PS}^2 = 2Bm_1$ holds. Then instead of m_i ($i=1,2$), one can use $m_{PS}(m_i, m_i)^2$ as the variable in the chiral extrapolation. For other hadrons, vector meson and octet and decuplet baryons, we also use the linear relations:

$$m_V(m_1, m_2) = m_V(0, 0) + B_V \cdot (m_1 + m_2), \quad (5.2)$$

$$m_{oct}(m_1, m_2, m_3) = m_{oct}(0, 0, 0) + B_{oct} \cdot (m_1 + m_2 + m_3), \quad (5.3)$$

$$m_{dec}(m_1, m_2, m_3) = m_{dec}(0, 0, 0) + B_{dec} \cdot (m_1 + m_2 + m_3). \quad (5.4)$$

The hadron spectrum and the result of fit are shown in Figure 10. The vertical axis is the averaged pseudoscalar meson mass squared,

$$\langle m_{PS}^2(m_i) \rangle = \frac{1}{N_q} \sum_{i=1}^{N_q} m_{PS}^2(m_i, m_i) = \frac{1}{N_q} \sum_{i=1}^{N_q} 2Bm_i \quad (5.5)$$

with $N_q = 2$ for mesons and $N_q = 3$ for baryons. The Λ -type baryon is not shown in the figure to avoid that the figure become too messy. The linear fit seems to be successful.

5.3 Spectrum at physical quark masses

To determine the hadron masses at the physical u , d and s quark mass, one need to set the scale of lattice. We do not distinguish the u and d quark masses, and express their mass as m_n . We adopt two definitions, through the hadronic radius r_0 , and through the K^* meson mass. These two methods are also adopted by UKQCD Collaboration in [15], and convenient for comparison of our data with theirs. In [15], they employed the values of clover coefficient determined in two ways: with nonperturbative renormalization technique (NP) [16], and tadpole-improvement (TAD) [12]. Then they extrapolate the masses to the continuum limit by simultaneous fit of these two types of data to the linear form in a^2 for NP and quadratic form in a for TAD. We compare our hadron spectrum at the physical quark masses with the result in the continuum limit of [15], although we ourselves do not perform the continuum extrapolation because of lacks of sufficient number of β as well as the statistical accuracy.

Scale set by r_0 . The hadronic radius r_0 has been already obtained in Section 4. The corresponding values of spatial lattice cutoff are found in Table 1. The PS meson masses squared correspond to m_n and m_s are then defined with $m_\pi^\pm = 139.6$ MeV and $m_K = 495.7$ MeV (isospin averaged), respectively. These definitions are in accord with [15]. The hadron masses extrapolated or interpolated to the physical points are shown in Figure 10 and listed in Table 11. For comparison with the result in [15], we also list the hadron masses multiplied by $r_0\xi$ in Table 11. In the latter case, ξ appears to multiply the quantity in the spatial lattice unit (r_0) to ones in the temporal lattice unit (masses). In our data, differences between the results at $\beta = 6.10$ and 5.95 rather large compared with the difference between $\beta = 5.95$ and 5.75. This would be partially due to the different a dependence of $O(\alpha a)$ and $O(a^2)$ lattice artifact, and also due to the statistical fluctuation. Our results of the meson masses seem to approach towards the continuum results by UKQCD Collaboration on the isotropic lattices [15].

Scale set by m_{K^*} . In the second case, $m_{K^*} = 893.9$ MeV (isospin averaged) is used to set the lattice scale. First we interpolate the vector meson mass to the point that the ratio of PS and

Table 11: Hadron spectrum for physical quark masses with the scale set by r_0 .

	mass [GeV]			$m\xi r_0$			Ref. [15]
	$\beta = 5.75$	$\beta = 5.95$	$\beta = 6.10$	$\beta = 5.75$	$\beta = 5.95$	$\beta = 6.10$	cont.
ρ	0.832(11)	0.846(17)	0.895(12)	2.105(28)	2.141(42)	2.265(30)	2.35(16)
K^*	0.9251(90)	0.938(13)	0.977(10)	2.342(23)	2.375(34)	2.473(25)	2.54(12)
ϕ	1.0185(71)	1.031(10)	1.059(8)	2.578(18)	2.610(26)	2.680(21)	2.729(77)
N	1.175(16)	1.155(22)	1.197(18)	2.974(40)	2.924(55)	3.032(45)	2.92(24)
Λ	1.260(13)	1.253(19)	1.283(16)	3.190(34)	3.172(47)	3.248(40)	3.22(20)
Σ	1.281(14)	1.268(19)	1.302(16)	3.242(35)	3.211(49)	3.295(41)	3.23(19)
Ξ	1.387(12)	1.381(17)	1.406(15)	3.510(31)	3.497(43)	3.558(37)	3.54(15)
Δ	1.403(28)	1.440(41)	1.521(41)	3.552(72)	3.65(10)	3.85(10)	3.86(37)
Σ^*	1.495(25)	1.532(36)	1.602(37)	3.784(63)	3.877(90)	4.055(93)	4.15(29)
Ξ^*	1.587(22)	1.623(31)	1.683(32)	4.017(54)	4.109(78)	4.260(81)	4.44(22)
Ω	1.679(18)	1.715(26)	1.763(28)	4.249(46)	4.341(66)	4.464(70)	4.72(17)

 Table 12: Hadron spectrum for physical quark masses with the scale set by m_{K^*} . The parameter J is also quoted, while it is dimensionless quantity.

	mass [GeV]			m/m_{K^*}			Ref. [15]
	$\beta = 5.75$	$\beta = 5.95$	$\beta = 6.10$	$\beta = 5.75$	$\beta = 5.95$	$\beta = 6.10$	cont.
ρ	0.796(11)	0.795(16)	0.802(11)	0.891(12)	0.890(18)	0.898(12)	0.921($^{+32}_{-56}$)
K^*	0.894(11)	0.894(16)	0.894(11)	–	–	–	–
ϕ	0.992(12)	0.993(16)	0.986(11)	1.109(13)	1.110(18)	1.103(12)	1.110($^{+8}_{-21}$)
N	1.125(15)	1.087(21)	1.075(16)	1.259(17)	1.216(23)	1.202(18)	1.14($^{+6}_{-18}$)
Λ	1.217(14)	1.194(20)	1.175(15)	1.361(15)	1.335(22)	1.315(17)	1.29($^{+5}_{-15}$)
Σ	1.236(14)	1.207(20)	1.191(16)	1.382(16)	1.351(23)	1.332(17)	1.29($^{+5}_{-14}$)
Ξ	1.346(14)	1.328(21)	1.307(15)	1.506(16)	1.485(23)	1.462(17)	1.45($^{+4}_{-10}$)
Δ	1.343(27)	1.354(39)	1.363(37)	1.502(30)	1.515(43)	1.525(41)	1.50($^{+17}_{-17}$)
Σ^*	1.439(25)	1.452(35)	1.454(33)	1.610(28)	1.624(39)	1.626(37)	1.64($^{+13}_{-13}$)
Ξ^*	1.535(23)	1.549(32)	1.544(29)	1.717(25)	1.733(36)	1.727(32)	1.79($^{+9}_{-10}$)
Ω	1.631(21)	1.647(30)	1.634(25)	1.825(24)	1.842(33)	1.828(28)	1.93($^{+7}_{-8}$)
J	0.3859(47)	0.3896(95)	0.3621(47)				

V meson masses is equal to the physical value of K^* and K mesons. Then this vector meson mass defines the lattice scale. This results in the spatial lattice cutoffs 1.053(13), 1.525(27) and 1.817(22) GeV at $\beta = 5.75$, 5.95 and 6.10, respectively. Then the values of m_{PS}^2 's correspond to the (u, d) and s quark masses are determined with experimental K and π meson masses. The hadron masses at physical quark masses are listed in Table 12. We observe similar tendency to the case of the scale set by r_0 . No signal of inconsistency with the result on isotropic lattice is found.

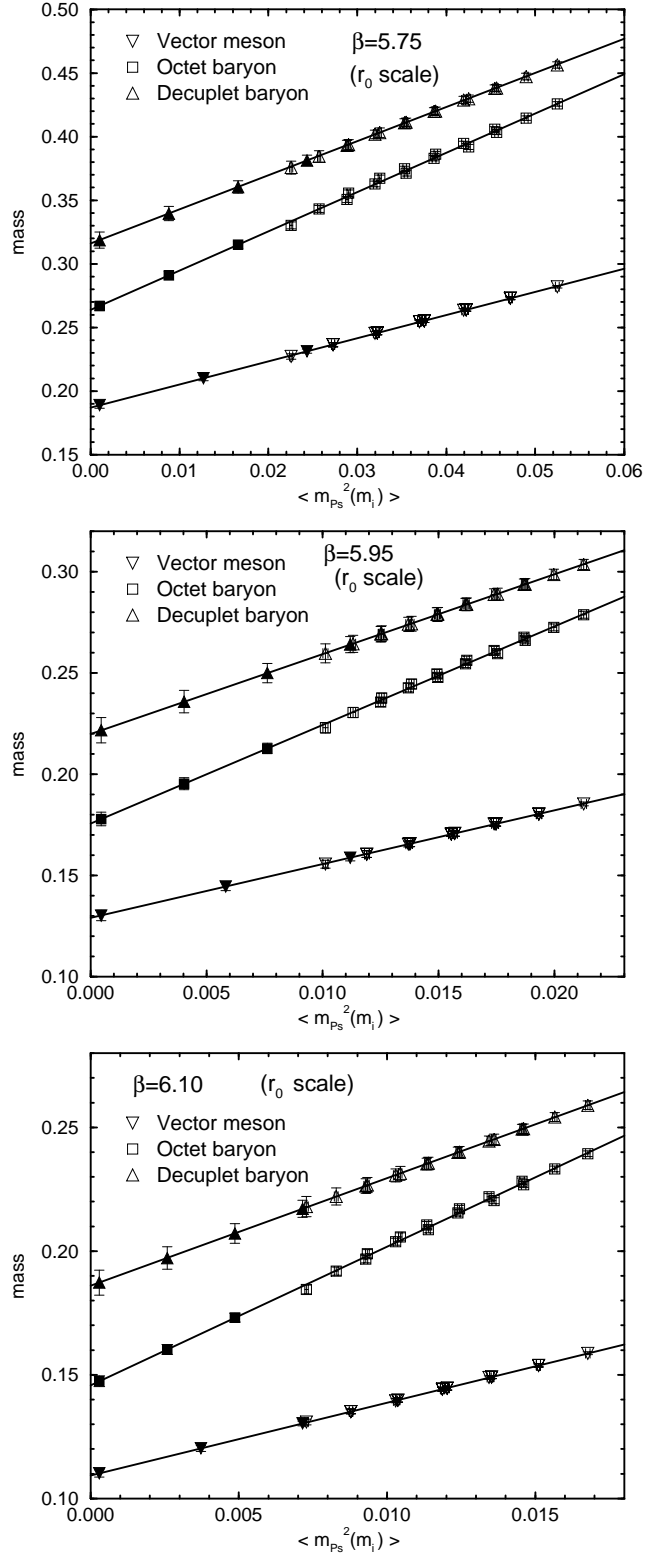


Figure 10: The masses of vector meson and the octet and decuplet baryons together with the result of linear fits. Only the Σ -type octet baryon is shown. The filled symbols corresponding to the masses at the physical u , d and s quark masses with the scale set by r_0 .

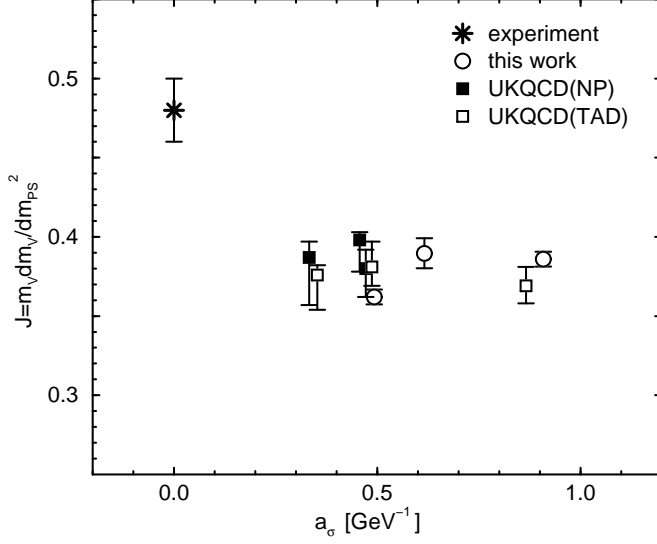


Figure 11: The parameter J . The a_σ is set by using r_0 . Data of UKQCD Collaboration (square symbols) are taken from Ref. [15] on the isotropic lattices, and slightly horizontally shifted.

5.4 J -parameter

The parameter J was introduced to probe the quenching effect in [17], and defined as

$$J = m_V \left. \frac{dm_V}{dm_{PS}^2} \right|_{m_V/m_{PS}=m_{K^*}/m_K}. \quad (5.6)$$

It is known that the quenched lattice simulation does not reproduce the experimental value, $J = 0.48(2)$, and gives about 20 % smaller value. We show our result of J in Figure 11, as the function of lattice spacing determined by r_0 . We find that our results are consistent to those by UKQCD on the isotropic lattices in the quenched approximation.

5.5 Covariance of correlators

Let us consider the pseudoscalar correlator:

$$\begin{aligned} C_{PS}(\mathbf{p}, t) &= \langle O_{PS}(x) O_{PS}^\dagger(0) \rangle \\ &\rightarrow \frac{Z^2(\mathbf{p})}{2E(\mathbf{p})} \exp(-E(\mathbf{p})t) \quad (\text{large } t) \end{aligned} \quad (5.7)$$

with $Z(\mathbf{p}) = \langle 0 | O(x) | PS(\mathbf{p}) \rangle$. Here we employ the covariant normalization. For the local pseudoscalar density operator $O(x) = \bar{q}(x) \gamma_5 q(x)$, if the Lorentz covariance is sufficiently restored, $Z(\mathbf{p})$ does not depend on the momentum \mathbf{p} . Then

$$R(\mathbf{p}) = \frac{E(\mathbf{p}) Z(\mathbf{p})^2}{m_{PS} Z(0)^2} \quad (5.8)$$

probes the restoration of covariance as the deviation from unity. In figure 12, we show the momentum dependence of $R(\mathbf{p})$ measured on $\beta = 5.95$ and 6.10. At each β , the quark mass is

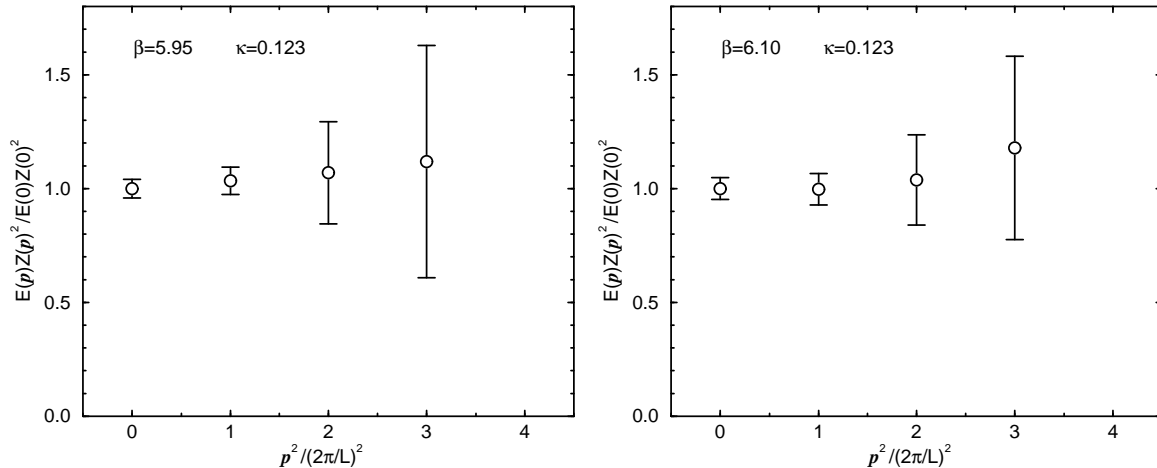


Figure 12: The covariance of the pseudoscalar correlators. The left figure is at $\beta = 5.95$ and $\kappa = 0.1230$, and the right one is at $\beta = 6.10$ and $\kappa = 0.1230$.

the largest one used in the light hadron spectroscopy. We find that $R(\mathbf{p})$ at finite momentum is consistent with $R(\mathbf{p} = 0)$, while higher momentum states suffer from large statistical fluctuation. This feature is particularly important in the calculation of form factors, in which the finite momentum states play an essential role.

5.6 Systematic errors of the spectrum from calibration

To estimate the systematic effect due to the uncertainty of calibration, we obtain the spectrum at the same κ 's with slightly shifted bare anisotropy, $\gamma'_F = \gamma_F^* + \delta\gamma_F$. We set $\delta\gamma_F = 0.1$, which implies about 2.5 % shift of bare anisotropy. Figure 13 shows the result for shifted γ'_F together with the result for γ_F^* , for $\beta = 5.75$ and 6.10. There are small systematic downward shifts in the fitted lines. The spectrum at the physical quark masses are listed in Table 13 as the dimensionless combination, $m\xi r_0$ and m/m_{K^*} . The difference between the masses with γ'_F and γ_F^* is slightly amplified toward the chiral limit. Even for the lightest mass in each species, the difference is at most around 1 %. This implies that the uncertainty of hadron masses at the physical (u, d) and s quark mass are about half of uncertainty in γ_F . With the relativistic dispersion relation, γ_F^* at $m_q = 0$ has been determined at each β within about 2 % ambiguity: the statistical error of 1 % and the systematic error of 1 % in the form of fit. Therefore there is 1 % level uncertainty in the hadron spectrum due to the uncertainty in calibration. This feature would make the anisotropic lattice promising for future physical applications.

6 Conclusion

In this paper, we studied the $O(a)$ improved quark action on the anisotropic lattice with anisotropy $\xi = a_\sigma/a_\tau = 4$. The bare anisotropy γ_F^* , with which $\xi_F = \xi$ holds, is determined for the whole quark mass region below the charm quark mass, including the chiral limit in 1 % statistical accuracy. In the massless limit, there is also about 1 % systematic uncertainty in extrapolating γ_F^* to $m_q = 0$.

The uncertainties in the calibration due to the discretization errors are studied by changing the physical inputs or conditions. (i) We have shown that the dispersion relations for the

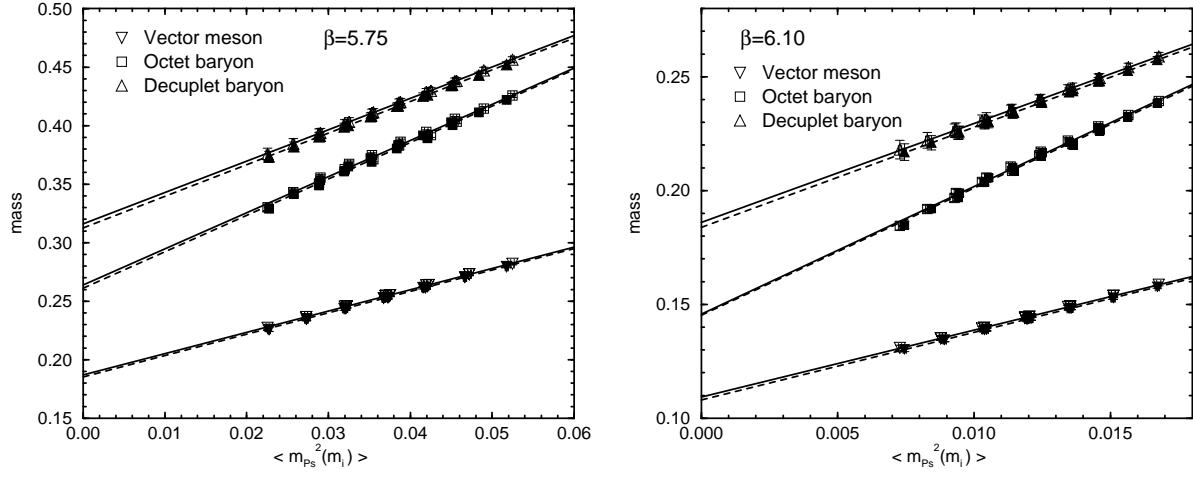


Figure 13: The spectra with shifted γ_F (filled symbols) together with the results at γ_F^* (open symbols). The solid lines and dashed lines represent the fit results at $\gamma_F = \gamma_F^*$ and $\gamma_F^* + \delta\gamma_F$, respectively.

Table 13: Spectra with shifted γ_F in the dimensionless combinations. The dimensionless parameter J is also listed.

β	$m\xi r_0$			m/m_K^*		
	5.75	5.95	6.10	5.75	5.95	6.10
ρ	2.084(26)	2.121(40)	2.239(28)	0.891(11)	0.890(17)	0.898(11)
K^*	2.322(21)	2.357(32)	2.448(24)	—	—	—
ϕ	2.560(17)	2.592(24)	2.658(19)	1.109(12)	1.110(17)	1.102(12)
N	2.946(37)	2.913(52)	3.019(43)	1.260(16)	1.223(22)	1.212(17)
Λ	3.166(32)	3.161(45)	3.236(38)	1.363(15)	1.341(21)	1.323(16)
Σ	3.216(33)	3.199(46)	3.282(39)	1.383(15)	1.356(22)	1.340(17)
Ξ	3.486(29)	3.485(41)	3.545(35)	1.507(15)	1.490(22)	1.468(17)
Δ	3.514(66)	3.614(96)	3.808(96)	1.503(28)	1.517(41)	1.527(38)
Σ^*	3.748(58)	3.847(85)	4.014(85)	1.610(26)	1.625(37)	1.627(34)
Ξ^*	3.983(50)	4.080(73)	4.221(75)	1.717(24)	1.734(34)	1.728(30)
Ω	4.217(43)	4.313(62)	4.427(65)	1.824(23)	1.842(32)	1.829(27)
J				0.3838(43)	0.3871(86)	0.3614(42)

pseudoscalar and the vector mesons give values of γ_F^* which differ by 1% at $\beta = 5.75$, while they show no difference at $\beta = 5.95$ and 6.10. (ii) Two different choices of the lattice dispersion relations, namely the naive continuum form and the Klein-Gordon form, also lead to the results which differ by 3% for $\beta = 5.75$, but we found no difference at $\beta = 6.1$ with $m_q < 0.2a_\tau^{-1}$. These systematic uncertainties tend to vanish toward the continuum limit.

The light hadron spectrum was studied using the central value of tuned bare anisotropy, $\gamma_F^*(m_q = 0)$. We found that it is consistent with the result on the isotropic lattice by UKQCD Collaboration. It was found that a change of γ_F^* by 2% would lead to a change of the spectrum by 1% for the physical quark masses. We also investigated the Lorentz invariance of the matrix element of the pseudoscalar operator as a consistency check.

The main disadvantage in using the anisotropic lattice would lie in the additional systematic uncertainty caused by the calibration. There are two types of errors in γ_F^* . The first type consists of the statistical error and the error in the chiral extrapolation, which was estimated to be 2 % level. The second type consists of $O(\alpha a)$ and $O(a^2)$ systematic uncertainties, which was estimated to be 4% at $\beta = 5.75$ and smaller for larger β . In total, there is 6 % ambiguity at $\beta = 5.75$, which corresponds to our coarsest lattice, and 2–3 % ambiguities at $\beta = 6.10$. The relative errors in hadron spectrum are half of those in γ_F^* . Since the contribution from the second types of error vanishes in the continuum limit, we expect to obtain the hadron spectrum to 1 % accuracy in the continuum limit. This result is encouraging for further applications. The anisotropic lattice would already be applicable to quantitative studies which requires a few percent accuracy. To achieve higher accuracy, nonperturbative tuning of the clover coefficients are required.

Since the range of quark masses where the systematic errors are under control covers the charm quark region, it is also important to apply the present anisotropic lattice simulation to the charmonium and D meson systems.

Acknowledgments

We thank J. Harada, A.S. Kronfeld, O. Miyamura, N. Nakajima, Y. Nemoto, H. Suganuma and T.T. Takahashi for useful discussions. The simulation has been done on NEC SX-5 at Research Center for Nuclear Physics, Osaka University and Hitachi SR8000 at KEK (High Energy Accelerator Research Organization). H. M. is supported by Japan Society for the Promotion of Science for Young Scientists. H. M. was also supported in the early stage of this work by the center-of-excellence (COE) program at RCNP, Osaka University. T. O. is supported by the Grant-in-Aid of the Ministry of Education No. 12640279. T. U. is supported by the center-of-excellence (COE) program at CCP, Tsukuba University.

References

- [1] F. Karsch, Nucl. Phys. B **205** (1982) 285.
- [2] G. Burgers, F. Karsch, A. Nakamura and I. O. Stamatescu, Nucl. Phys. B **304** (1988) 587.
- [3] M. Fujisaki *et al.* (QCD-TARO Collaboration), Nucl. Phys. B (Proc. Suppl.) **53** (1997) 426.
- [4] F. Karsch, J. Engels and T. Scheideler, Nucl. Phys. B (Proc. Suppl.) **63** (1998) 427; J. Engels, F. Karsch and T. Scheideler, Nucl. Phys. B **564** (2000) 303.
- [5] T. R. Klassen, Nucl. Phys. B **533** (1998) 557.
- [6] T. Umeda, R. Katayama, O. Miyamura and H. Matsufuru, Int. J. Mod. Phys. A **16** (2001) 2215.
- [7] T. R. Klassen, Nucl. Phys. B (Proc. Suppl.) **73** (1999) 918.
- [8] P. Chen, hep-lat/0006019.
- [9] CP-PACS Collaboration (A. Ali Khan *et al.*), Nucl. Phys. B (Proc. Suppl.) **94** (2001) 325.
- [10] J. Harada, A. S. Kronfeld, H. Matsufuru, N. Nakajima and T. Onogi, hep-lat/0103026.

- [11] A. X. El-Khadra, A. S. Kronfeld and P. B. Mackenzie, Phys. Rev. D **55** (1997) 3933.
- [12] G. P. Lepage and P. B. Mackenzie, Phys. Rev. D **48** (1993) 2250.
- [13] B. A. Thacker and G. P. Lepage, Phys. Rev. D **43** (1991) 196.
- [14] R. Sommer, Nucl. Phys. B **411** (1994) 839.
- [15] K. C. Bowler *et al.* (UKQCD Collaboration), Phys. Rev. D **62** (2000) 054506.
- [16] M. Lüscher, S. Sint, R. Sommer, P. Weisz and U. Wolff, Nucl. Phys. B **491** (1997) 323.
- [17] P. Lacey and C. Michael (UKQCD Collaboration), Phys. Rev. D **52** (1995) 5213.